AIAA 2003-1982

Prediction of Wrinkle Amplitudes in Square Solar Sails

Y.W. Wong and S. Pellegrino
University of Cambridge, Cambridge, CB2 1PZ, UK
K.C. Park
University of Colorado, Boulder, CO 80309-0429

44th AIAA/ASME/ASCE/AHS/ASC Structures, Structural Dynamics, and Materials Conference
7-10 April 2003
Norfolk, VA

Prediction of Wrinkle Amplitudes in Square Solar Sails

Y.W. Wong* and S. Pellegrino†
University of Cambridge, Cambridge, CB2 1PZ, UK
K.C. Park‡
University of Colorado, Boulder, CO 80309-0429

This paper considers an idealised solar sail consisting of a uniform, elastic, isotropic square membrane that is prestressed by two pairs of equal and opposite forces applied at the corners. Two wrinkling regimes are identified. The first regime occurs for symmetric and moderately asymmetric loading; it is characterised by small, radial corner wrinkles. The second regime occurs for strongly asymmetric loading and is characterised by a single, large diagonal wrinkle, plus small radial corner wrinkles. An analytical method for predicting wrinkle wavelengths and out-of-plane wrinkle displacements, as well as in-plane corner displacements of the membrane, is presented. The analytical predictions are validated against experimental measurements and detailed finite element simulation results. The accuracy achieved is typically better than 20% on wavelengths and 30% on amplitudes. Finite element analysis using thin shell elements is shown to be able to replicate real physical experimentation with an accuracy better than 20%.

Introduction and Background

It is envisaged that ultra-lightweight solar sails will be used as future interstellar probes, and several studies of these structures are currently underway [1]. One of the concepts proposed is the so-called suspension system in which a square sail with load carrying membranes is prestressed by applying concentrated corner forces by means of four deployable booms [2].

Stressing the membrane in uniform biaxial tension everywhere, which would completely avoid the formation of wrinkles, is not practical. Instead, many studies currently under way assume that extensive parts of the membrane will be stressed only uniaxially and hence will be subject to wrinkling. The magnitude of these structural wrinkles is of great interest to designers of solar sails, as the membrane reflectivity is a function of the wrinkle wavelength and amplitude; hence, depending on their geometric characteristics, wrinkles may or may not be acceptable.

This paper considers an idealised solar sail consisting of a uniform elastic square membrane of side length L and thickness t that is prestressed by two pairs of equal and opposite concentrated forces, T_1 and T_2, applied at the corners, as shown in Figure 1. The membrane is isotropic with Young's Modulus E and Poisson's ratio ν; it is also initially stress free and perfectly flat (before the application of the corner forces).

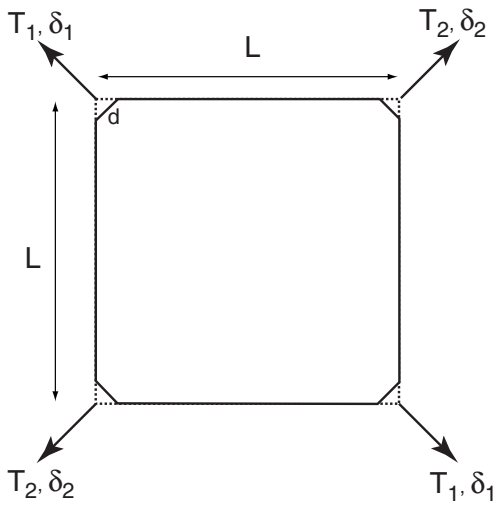

Fig. 1 Membrane subjected to corner forces.

An analytical method is presented for estimating the wrinkle patterns in this membrane, and their amplitude and wavelength, induced by the general loads T_1 and T_2. Predictions from the proposed method are validated against experimental measurements and detailed finite element simulation results. This method is an extension of our previous paper on long, rectangular membranes under uniform shear [3]. In the previous study the wrinkles in the central region were parallel, uniform, and at 45° to the edges of the membrane. The mid-plane stress along the wrinkles (tensile) could be assumed to be uniform and hence could be expressed in terms of the applied shear. The mid-plane stress

*Research Student, Department of Engineering, Trumpington Street.
†Professor of Structural Engineering, Department of Engineering, Trumpington Street. Associate Fellow AIAA. pellegrino@eng.cam.ac.uk
‡Professor, Center for Aerospace Structures and Department of Aerospace Engineering Sciences, UCB 429. Associate Fellow AIAA.

transverse to the wrinkles (compressive) was set equal to the buckling stress of an infinitely wide plate in uniaxial compression —which, of course, depends on the bending stiffness of the plate. Finally, the unknown buckling wavelength of this plate was obtained from an equation of out-of-plane equilibrium for the wrinkled, and hence doubly-curved, membrane.

A key difficulty in extending this previous work to square membranes is that it is now much more difficult to guess a reasonably accurate stress field. Hence we propose four different, no-compression "equilibrium" stress fields, some of which are only valid if the ratio of the corner forces is in a particular range. Each stress distribution is associated with a particular upper-bound estimate of the corner displacements due to the corner forces. Hence, if for a given load ratio and membrane dimensions there is more than one potential stress distribution, the best approximation to the actual stress field in the membrane is obtained by choosing the particular distribution that produces the lowest upper bound for the corner deflections.

Once a good approximation to the stress field has been identified, the corresponding wrinkle details are predicted by an extension of the approach proposed in our previous paper [3]. Results from this approach are compared both to experimental measurements and very detailed non-linear finite element simulations based on the technique first developed in Ref. [4].

Analytical Model: Stress Field

Figure 2 shows four possible stress fields, all of which satisfy equilibrium everywhere and involve no compressive stress at any point. Note that in each case the membrane is divided into regions which are either unloaded or subject to a simple state of stress. Also note that the stress field in Figure 2(b) is valid only for $T_1 = T_2$ while the others are more general, although still subject to some restrictions as explained later.

Although equilibrium is satisfied, there is no guarantee that the elastic strains associated with these fields are compatible; indeed obvious compatibility violations can be easily detected for the simpler fields. Finally, note that the corner forces are distributed over a finite width, d, otherwise infinite stresses would occur. In a real solar sail, this width would be related to the size of the boom attachment to the membrane.

For each stress field it is possible to produce an estimate of the corresponding corner displacements, δ_1 and δ_2, defined in Figure 1. These displacements are computed using an upper-bound approach based on the complementary strain energy in the membrane.

The theorem of minimum complementary energy states that the total complementary energy in a linear-elastic structure is minimum for the actual stress distribution. Hence, for an assumed stress field —which satisfies equilibrium but not necessarily compatibility— the complementary energy will be higher than for the actual stress distribution [5]; thus

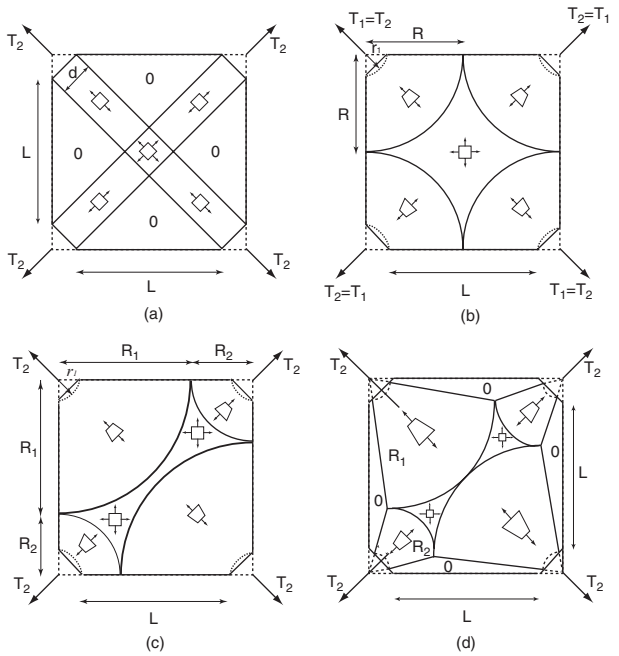

Fig. 2 Equilibrium stress fields.

$$U \leqslant U^* \tag{1}$$

where U and U^* are the actual and the estimated complementary energies of the structure. Hence, the "best" stress field is that which produces the smallest estimate of U^*.

U^* can be calculated from

$$U^* = \frac{1}{2}\int_V (\epsilon_1\sigma_1 + \epsilon_2\sigma_2)dV \tag{2}$$

By conservation of energy, U is given —for two given sets of corner forces, T_i and corresponding corner displacements δ_i— by

$$U = \frac{1}{2}\sum_{i=1}^{2} 2T_i\delta_i = T_1\delta_1 + T_2\delta_2 \tag{3}$$

Hence, from Equation 1, the average of the corner displacements, each weighted by the corresponding applied forces, determined by means of this method, is always an upper bound to the correct value.

Diagonal Strip Field

Figure 2 (a) shows a very simple stress field, consisting of two diagonal tension strips of width d, each under uniform uniaxial stress, plus a small isotropic biaxial stress in the centre region. The remaining parts of the membrane are unstressed. Figure 3 shows the stress distribution in a quarter of the structure.

For the case of symmetric loading, $T_1 = T_2 = T$ and $\delta_1 = \delta_2 = \delta$, the uniaxial stress in the tension strips is

$$\sigma_t = \frac{T}{dt} \tag{4}$$

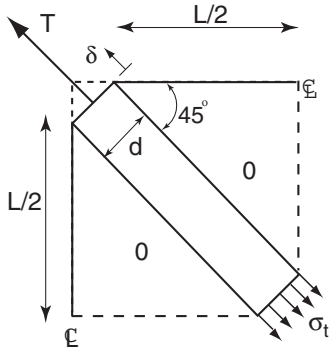

Fig. 3 Diagonal tension strip stress field.

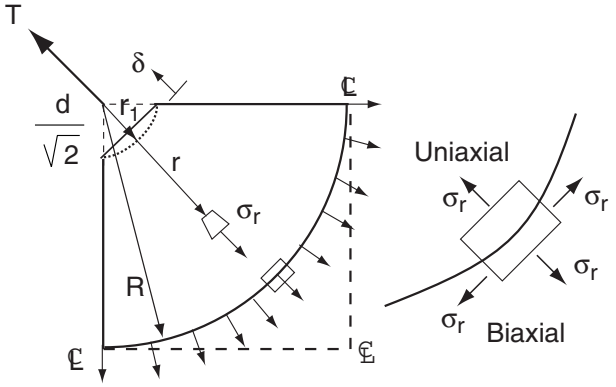

Fig. 4 Corner wedge stress field.

the complementary strain energy in each diagonal region is

$$U_1^* = \frac{T^2 L}{2\sqrt{2}dEt} \tag{5}$$

whereas the complementary strain energy in the central region is

$$U_2^* = \frac{T^2(1-\nu)}{4Et} \tag{6}$$

Hence, the corner displacement, δ, determined from Equations 1, 3, 5 and 6 is

$$\delta \leqslant \frac{T}{2Et}\left[\frac{\sqrt{2}L}{d} + (1-\nu)\right] \tag{7}$$

Corner Wedge Field

The second stress field, shown in Figure 2(b), consists of four identical corner regions subject to purely radial stress plus a central region under uniform biaxial stress. For simplicity, a symmetric load case, $T_1 = T_2 = T$ and $\delta_1 = \delta_2 = \delta$, will be considered first. A detailed view is shown in Figure 4.

The corner region stress distribution is chosen to be

$$\sigma_r = \frac{T}{\sqrt{2}rt} \tag{8}$$

at distance $r < \frac{L}{2}$ from the apex. Hence, the radial stress is uniform on any circular arc; all other stress components are zero. It can be readily shown that this distribution satisfies equilibrium.

To avoid stress singularities it is assumed that the force T is distributed over a small, biaxially stressed corner region of radius, $r_1 = \frac{d}{\sqrt{2}}$. Here the stress is given by Equation 4.

The central region, defined by circular arcs of radius $R = \frac{d}{\sqrt{2}} + \frac{L}{2}$, is subject to uniform biaxial stress of magnitude

$$\sigma_R = \frac{\sqrt{2}T}{(\sqrt{2}d + L)t} \tag{9}$$

The total complementary energy for all these regions is

$$U^* = \frac{T^2}{8Et}\left(\pi \ln\left|\frac{R}{r_1}\right| + 2(1-\nu)\right) \tag{10}$$

From which, expressing R and r_1 in terms of L and d, the following upper bound for δ is obtained

$$\delta \leqslant \frac{T}{4Et}\left[\pi \ln\left|1 + \frac{L}{\sqrt{2}d}\right| + 2(1-\nu)\right] \tag{11}$$

This type of stress field can be extended to asymmetric loading. For example, consider what happens if —starting from the symmetric case described above— T_1 is gradually increased. For equilibrium, we need to ensure that the radial stress is uniform on the four arcs bounding the central region. Since σ_r in each wedge region is proportional to T_i/r, we can compensate for the increase in T_1 by increasing the outer radius of this wedge and decreasing the radius of the wedge corresponding to T_2. For the radial stress along the edges of the centre region to be uniform, clearly $R_1/R_2 \propto T_1/T_2$. This approach is valid until the two larger arcs reach the centre of the membrane, which happens for

$$\frac{R_1}{R_2} = \frac{T_1}{T_2} = \frac{1}{\sqrt{2}-1} \tag{12}$$

By dividing the stress field shown in Figure 2(c) into separate regions, each contributing to the complementary strain energy associated with the displacement in only one direction, two separate estimates can be obtained. Thus,

$$\delta_1 \leqslant \frac{T_1}{4Et}\left[\pi \ln\left|\frac{R_1}{r_1}\right| + \frac{1-\nu}{R_1^2}\left(4R_1R_2 - 2R_2^2\right)\right] \tag{13}$$

and an analogous expression for δ_2.

Modified Corner Wedge Field

As we have stated earlier, the corner wedge stress field is only valid up to a specific value of T_1/T_2. We have observed that around this value there is a fairly sudden change in the wrinkling pattern of the membrane, involving the formation of a diagonal wrinkle. For such a wrinkle to form, there has to exist a region —continuous between the two most heavily loaded corners of the membrane— with no tensile transverse

stress. This can be achieved by varying the angle subtended by each corner wedge, as shown in Figure 2(d) and 5. Note that the half-angles defining the corner wedges are θ_1, θ_2 and the unstressed triangular region is defined by the angles α_1, α_2.

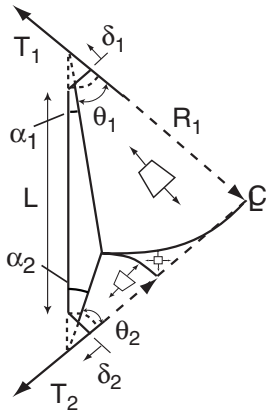

Fig. 5 Modified corner wedge stress field.

The radial stress is now given by

$$\sigma_r = \frac{T_i}{2rt\sin\theta_i} \tag{14}$$

and hence along the circular arcs that bound the central, biaxially stressed region,

$$\sigma_r = \frac{T_1}{2R_1 t\sin\theta_1} = \frac{T_2}{2R_2 t\sin\theta_2} \tag{15}$$

Given T_1 and T_2, one can find by geometry, plus Equation 15, a unique set of θ_1, θ_2 and R_1, R_2, thus fully defining the stress field.

Note that α_i is related to θ_i by

$$\theta_i = 45^\circ - \alpha_i \tag{16}$$

It should be noted that θ_1 and θ_2 are constant for any particular load ratio, and so the only variable in Equation 14 is r. Hence, this field is different from any of the others, as the slack regions, denoted by 0 in Figure 5, will grow as the load ratio is increased.

By an extension of the approach described previously, we can obtain the following expression for an upper bound on the corner displacements

$$\delta_i \leqslant \frac{T_i}{2Et\sin^2\theta_i}\left[\theta_i \ln\left|\frac{R_i}{r_1}\right| + (1-\nu)\left(\frac{A}{R_i^2} + \theta_i - \frac{1}{2}\tan\theta_i\right)\right] \tag{17}$$

where A is the area of the central, biaxially tensioned region. However, note that δ_2 obtained from this equation does not allow for the geometric effects associated with the wrinkling the membrane, which are quite large since $T_1 >> T_2$.

Analytical Model: Wrinkle Details

The simple analytical model recently developed by Wong and Pellegrino [3] to predict the wrinkle wavelength and amplitude in a sheared rectangular membrane will be extended to the present situation. A key assumption of this model is that a critical transverse compressive stress must be reached when wrinkling occurs in the membrane. This critical stress, $\sigma_{\rm cr}$, is equal to the buckling stress of a plate of wavelength λ in the direction perpendicular to the wrinkles and is given by

$$\sigma_{\rm cr} = -\frac{\pi^2}{\lambda^2}\frac{Et^2}{12(1-\nu^2)} \tag{18}$$

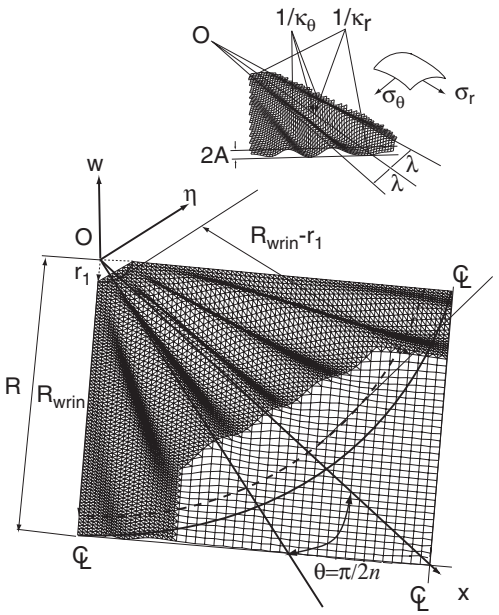

Fig. 6 Wrinkle detail at a corner.

This stress has to satisfy out-of-plane equilibrium in a wrinkled membrane that carries along the wrinkles the stress provided by one of the stress fields proposed in the previous section.

Figure 6 shows the corner wrinkle details in a quarter of a symmetrically loaded square membrane. Note that the wrinkles radiate outwards, instead of being uniform as in the rectangular membrane under shear. Let us denote by R_{wrin} the outer radius of the wrinkled zone, see Figure 6. It is assumed that the wrinkles start growing right at the edge of the highly stressed corner region. The wrinkle profile is assumed to have attained its maximum amplitude in the middle but, of course, the wrinkle becomes wider as r increases. Using the polar coordinate system defined in Figure 6, the out-of-plane displacement of the membrane is assumed to be

$$w \approx A\sin\frac{\pi r}{R_{wrin} - r_1}\sin 2n\theta \tag{19}$$

where A is the wrinkle amplitude, n the total number of wrinkles at the corner —each subtending an angle

of $\pi/2n$— and θ is an angular coordinate measured form the centre line.

Two sets of predictions will be developed for two different loading regimes of the membrane. The diagonal strip stress field gives poor estimates of the corner displacements, hence no further analysis of this field will be carried out.

Symmetric Loading

Consider the corner wedge stress field. Since the stress is uniaxial

$$\epsilon_r = \frac{\sigma_r}{E} \tag{20}$$

where σ_r is given by Equation 8. The radial displacement, $u(r)$, can be obtained by integrating the radial strain along the radius

$$u = \int \epsilon_r dr + c \tag{21}$$

where c is a constant of integration such that $u \approx 0$ at $r = R$, i.e. where the stress distribution becomes biaxial. Therefore,

$$u = \frac{1}{\sqrt{2}Et} \ln \frac{r}{R} \tag{22}$$

The hoop strain required for geometric compatibility is

$$\epsilon_{\theta_g} = -\epsilon_r = -\frac{u}{r} \tag{23}$$

On the other hand, the hoop material strain is

$$\epsilon_{\theta_m} = -\nu \frac{\sigma_r}{E} \tag{24}$$

Wrinkles will form when the geometric hoop strain is larger than the material strain, hence from Equations 8, 22, 23 and 24, we obtain

$$\ln \left| \frac{R}{r} \right| \geq \nu \tag{25}$$

In order for wrinkles to form Equation 25 must be satisfied, hence the largest r for which the equation is satisfied is R_{wrin}. For $r < R_{wrin}$, any mismatch in the strain will require a "wrinkling" strain achieved by out-of-plane displacement of the membrane

$$\epsilon_{\theta_g} = \epsilon_{\theta_m} + \epsilon_{\theta_{wrin}} \tag{26}$$

Hence at a general $r < R_{wrin}$

$$-\frac{u}{r} = -\frac{\nu T}{\sqrt{2}rEt} + \frac{a^2\pi^2}{4\lambda^2} \tag{27}$$

where $a = A \sin \pi r/(R_{wrin} - r_1)$.

Now, consider out-of-plane equilibrium of the wrinkled membrane

$$\sigma_r \kappa_r + \sigma_\theta \kappa_\theta = 0 \tag{28}$$

where κ_r and κ_θ are the radial and hoop curvatures, respectively, obtained by differentiating w in Equation 19. Hence,

$$\kappa_r = \frac{A\pi^2}{(R_{wrin} - r_1)^2} \quad \text{and} \quad \kappa_\theta = \frac{4An^2}{r^2} \tag{29}$$

It is found that the number of half-wave wrinkles at a distance r from the membrane corner is given by

$$n = \sqrt[4]{\frac{3\pi^2(1-\nu^2)Tr^3}{4\sqrt{2}Et^3(R_{wrin} - r_1)^2}} \tag{30}$$

and hence we can determine the wavelength at any r by substituting n from Equation 30 into

$$\lambda = \frac{r\pi}{2n} \tag{31}$$

Once the wavelength has been determined, it is then possible to predict the average wrinkle amplitude $a(r)$ using Equations 23 to 26. Thus

$$a = \frac{2\lambda}{\pi} \sqrt{\frac{u}{(r - r_1)} + \frac{\nu T}{\sqrt{2}rEt}} \tag{32}$$

Note that Equation 32 is only valid for $r \leqslant (R_{wrin} - r_1)/2$ and the amplitude beyond this value of r is obtained by considering the mirror image.

It is straightforward to extend the predictions discussed above to the more general case $1 < T_1/T_2 < 1/(\sqrt{2} - 1)$.

Asymmetric Loading

For higher load ratios, two wrinkle regions develop. One is similar to the previous case, i.e. a fan of wrinkles originating from a corner. The other and much more dominant is a single wrinkle running along the diagonal axis of the membrane, and going through the narrow region where the two larger wedge stress fields come into contact, see Figure 2(d). We will only predict the wavelength and amplitude of this diagonal wrinkle as its amplitude is much larger than the rest of the wrinkles in the corner.

The diagonal wrinkle can be described by the simple mode shape

$$w = A \sin \frac{\pi\xi}{\sqrt{2}L - 2r_1} \sin \frac{\pi\eta}{\lambda} \tag{33}$$

where λ is the half-wavelength, and A the maximum amplitude. The ξ, η coordinate system is shown in Figure 6.

The stress along the wrinkle is given by Equation 14, and the corresponding corner deflections, δ_1 and δ_2, from Equation 17.

To compute the amplitude of this single diagonal wrinkle we cannot proceed as before, because the diagonal parallel to T_2 is mostly straight with only a single large wrinkle in the middle. Hence, instead of

working in terms of average strains, here we work in terms of the total extension of this diagonal. We begin by noting that the modified corner wedge stress field involves slack regions along the edges of the membrane. If these regions do not deform out of plane, the edges of the membrane sides would behave as four rigid links, and hence the corners where T_2 is applied would move inwards by δ_1. Hence, denoting by e the extension of this diagonal

$$e = -2\delta_1 \tag{34}$$

This extension includes a component due to elastic stretching of the material, e_M, which can be obtained by integrating the elastic strains along this diagonal, over the uniaxially and biaxially stressed regions, from one corner to the other. Plus, a geometric shortening due to a single wrinkle, e_{wrin}. Hence

$$e = e_M - e_{wrin} \tag{35}$$

Substituting appropriate expressions

$$-2\delta_1 = 2\delta_2 - \frac{\nu T}{Et\sin\theta_i}\ln\left|\frac{R_1}{R_2}\right| - \frac{A^2\pi^2}{2\lambda} \tag{36}$$

The wrinkle half-wavelength is obtained by substituting the longitudinal and transverse curvatures — obtained by differentiating Equation 33— into an equilibrium equation analogous to Equation 28. Hence,

$$\lambda = \sqrt[4]{\frac{2\pi^2(R_i - r_1)^2 Et^3 r\sin\theta_i}{3(1-\nu^2)T}} \tag{37}$$

Substituting into Equation 36 and rearranging gives

$$A = \frac{1}{\pi}\sqrt{2\lambda\left(2(\delta_1+\delta_2) - \frac{\nu T}{Et\sin\theta_i}\ln\left|\frac{R_1}{R_2}\right|\right)} \tag{38}$$

where δ_1 and δ_2 come either from Equation 17 or from a FE estimate, as we will see later.

Comparison with FE Simulations

Several simulations have been conducted of a 500 mm square Kapton membrane with the following properties: E=3530 N/mm^2, $v = 0.3$, $t = 0.025$ mm, and $d = 25$ mm.

Different combinations of corner loads were considered. One quarter of the finite element model is shown in Figure 7. A very dense mesh was chosen after several preliminary analyses, in order to capture the fine wrinkle details in the corners. Other details of the FE model include a 25 mm × 20 mm Kapton reinforcement in each corner with a thickness of 0.1 mm, connected to a beam that distributes the applied corner load.

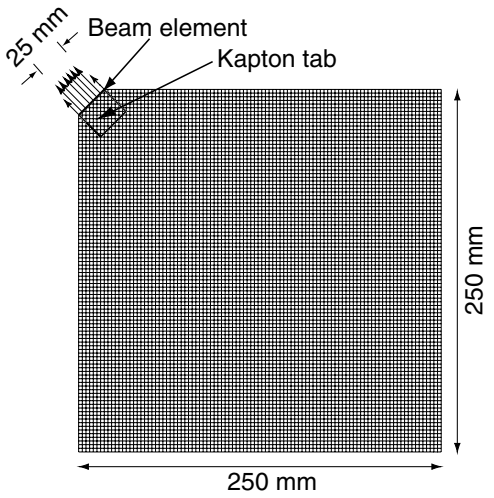

Fig. 7 1/4 of FE model.

Finite Element Model

The present authors have already shown that wrinkling of a thin membrane can be accurately modelled using thin shell elements, by introducing an initial geometrical imperfections obtained from an initial eigenvalue analysis. A geometrically non-linear post-wrinkling analysis is then carried out using the automated pseudo-dynamic *STABILIZE function in ABAQUS [6].

This method, although expensive in computational terms, is thus far the only method that can reveal full wrinkle details and can be relied upon as an almost exact replication of physical experimentation.

However, a simpler way of simulating membrane wrinkling is by means of a two-dimensional membrane made of no-compression material. This option is also available in ABAQUS. However, it is well known that wrinkled membranes are best described by combined stress-strain criteria, and Adler [7] has recently developed an ABAQUS user subroutine which models wrinkling by means of an Iterative Modified Properties (IMP) method.

Both of these FE modelling techniques have been used to find reference values for the corner displacements which could be compared against those from the simple analytical expressions proposed in the previous section.

Simulation Details

The membrane and corner tabs were modelled using S4R5 thin shell elements with different thicknesses, whereas the beam was modelled using a "Circ" general beam section. The boundary conditions are that the membrane is only constrained in the x and y directions at the centre, with all side edges remaining free; the out-of-plane and all bending degree of freedoms of the corner beams were restrained. The corner tensions were applied as distributed loads along the

truncated corners. For the IMP model, the membrane was modelled using M3D4 membrane elements, with material definition through a UMAT subroutine. The corner tab was modelled using S4 shell elements and the same beam elements used for the shell model.

Two load steps were applied, first a symmetric loading of 5 N at all corners. Then, the T_2 was maintained constant at 5 N while T_1 was increased up to 20 N, to obtain a final load ratio of $T_1/T_2 = 4$.

The analysis procedure was essentially identical for all the simulations. First, a uniform stress of 0.5 N/mm^2 was applied to provide an initial out-of-plane stiffness to the membrane. This was achieved by using *INITIAL CONDITION, TYPE=STRESS command in ABAQUS. A non-linear geometry analysis with *NLGEOM then followed to check the equilibrium of the system after this initial prestress had been applied.

Then a linear eigenvalue analysis step was carried out (for the thin shell model only) in order to extract possible wrinkling mode-shapes of the membrane under a symmetrical loading. These mode-shapes were selected based on their resemblance to the expected final wrinkled shape, and were introduced as initial geometrical imperfections.

Finally, an automatically stabilised post-wrinkling analysis was performed with the aid of *STATIC, STABILIZE. Since this analysis is very sensitive and the magnitude of wrinkles is very small, an increment of 0.001 of the total load had to be selected. The stabilize factor was reduced to 10^{-12} to minimise its effect on the final solution, but enough to stabilise the solution.

Symmetric Loading

Figure 8 shows a non-dimensional plot of the corner displacements predicted using different solutions methods for a symmetrically loaded membrane.

The plot shows a linear relationship between the corner displacement and the applied load. Also, all displacements predicted analytically are greater than the ABAQUS estimates, as expected. Note that Equation 11 gives closer predictions than Equation 7 which indicates that the corresponding stress field is more accurate.

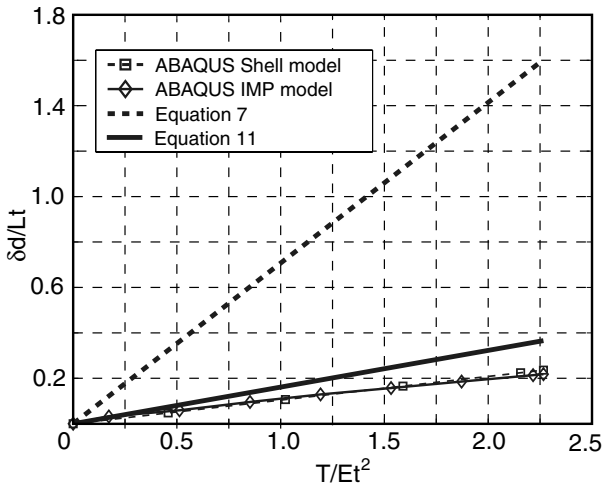

Fig. 8 Comparison of corner displacement for $T_1 = T_2 = T$.

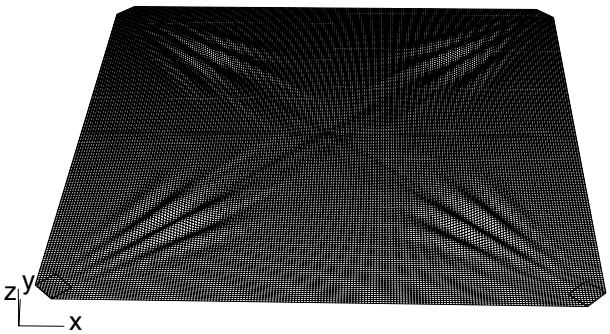

Fig. 9 Wrinkled shape for $T_1/T_2 = 1$.

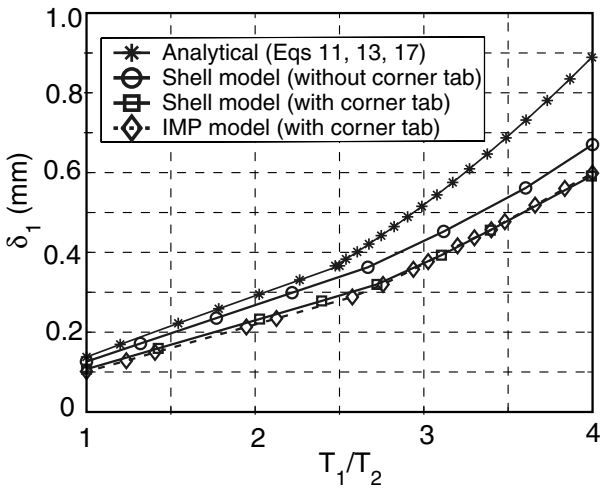

Fig. 10 Comparison of corner displacement for asymmetric loading.

Figure 9 shows the wrinkled shape of the membrane loaded by $T_1 = T_2 = 5$ N. The wrinkle amplitudes are very small and symmetrically arranged. The out-of-plane deformation of this plot has been scaled up 100 times for clarity.

Asymmetric Loading

Asymmetric load cases were simulated by first loading the membrane symmetrically with 5 N, then T_1 was increased up to a ratio of $T_1/T_2 = 4$.

Comparisons of corner displacements obtained by the two FE techniques and those predicted from Equations 13 and 17 are presented in Figure 10. Equation 7 has not been plotted because it generally over predicts the deflections by a factor of 2.

The main observation is that the membrane behaves linearly up to a load ratio of approximately 2.6, at which point its stiffness along the main diagonal sud-

denly decreases by about a third, as shown by the gradient of both the shell and IMP model solutions. This may be due to the formation of a large diagonal wrinkle. The standard membrane solution does not show this stiffness drop, and hence carries on linearly.

Note that the deflection estimates using Equations 13 and 17 provide a fairly close approximation to the corner displacements. Also note that the analytical estimates become more accurate if compared to a FE simulation without the corner tabs, which are not included in the analytical solution.

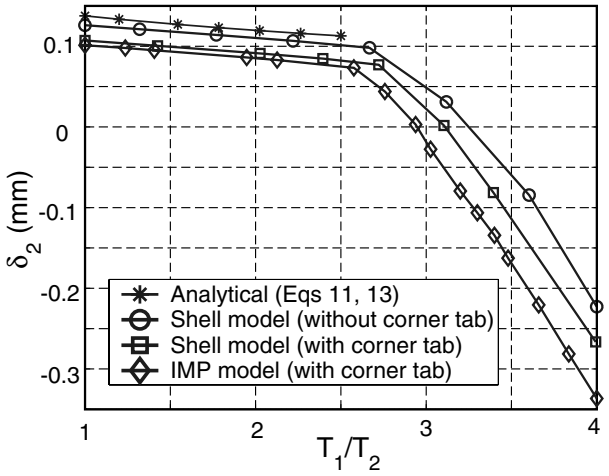

Fig. 11 Comparison of corner displacement for asymmetric loading.

Similar behaviour is observed for the lightly loaded corners. It can be seen that δ_2 decreases when the load ratio is increased, and the rate of decrease is much greater beyond a load ratio of 2.6. Equation 13 follows the response path very accurately up to its limit of validity. It is interesting to note that the IMP model tends to deflect more than the shell model, because it neglects the bending stiffness of the wrinkled membrane.

At this stage we will not extend the analytical estimates beyond $T_1/T_2 = 1/(\sqrt{2}-1)$, as we have already succeeded in showing that the proposed stress fields provide reasonably good approximations to the stresses in an actual wrinkled membrane.

Figure 12 shows the wrinkled shape of a membrane subjected to an asymmetric loading with $T_1/T_2 = 4$. In addition to the larger diagonal wrinkles between the more heavily loaded corners, a number of wrinkles of small amplitude can also be seen near the other corner.

Comparison with Experimental Observations

Careful experimental measurements were made, using a CCD laser, on a Kapton membrane with the properties defined in the previous section.

First, we increased the loading symmetrically. We started by applying 5 N, then 10 N and finally 20 N. An

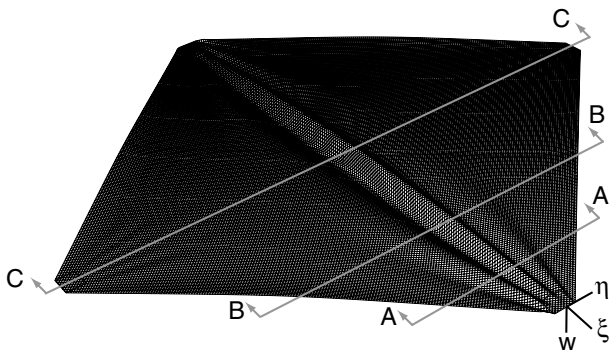

Fig. 12 Wrinkle details for $T_1/T_2 = 4$.

interesting observation was that the wrinkle pattern and the wrinkled region remained essentially the same under these different load levels. Mode jumping, first observed by the current authors [3, 4] in membranes under simple shear, occurred also in this experiment.

Photographs of the wrinkle patterns under symmetric and asymmetric loading are presented in Figure 13. For symmetric loading, Figure 13(a), the wrinkle pattern is fairly symmetric with wrinkles radiating outward from all the corners; a central region which is visibly stressed biaxially is free of wrinkles. For load ratios up to $T_1/T_2 = 2$ the wrinkles form only radially outwards at the corners, as expected. Then, for $T_1/T_2 = 3$ a large diagonal wrinkle is clearly visible, as predicted by the stress field approach.

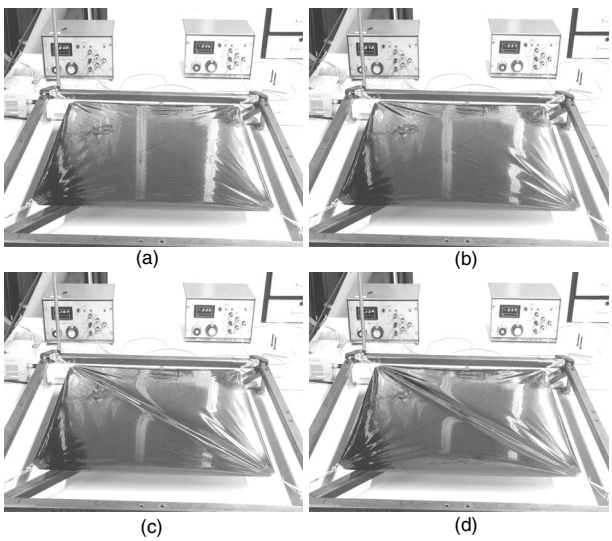

Fig. 13 Shapes of membrane for T_1/T_2 equal to (a) 1, (b) 2, (c) 3, (d) 4.

Detailed measurements of the wrinkle profile for symmetric loading show that the wrinkle amplitude increases as one moves away from the corner and reaches a maximum at a distance of 105 mm from the corner. The wrinkles have almost vanished at a distance of about 180 mm. There is little change when the loads are increased, however the number of wrinkles

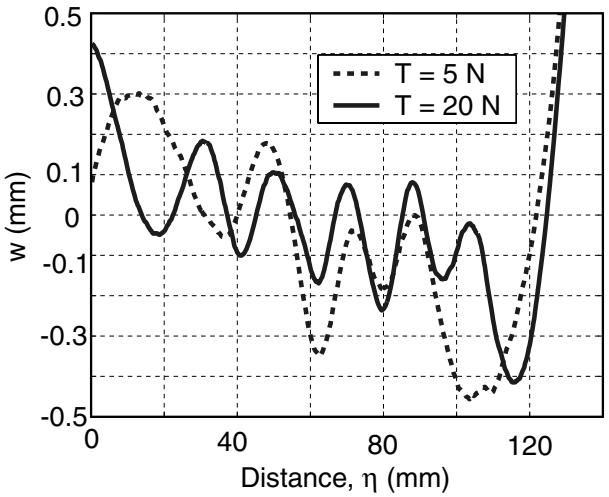

Fig. 14 Wrinkle profile at 70 mm from highly loaded corner, for $T_1 = T_2 = T = 5$ N and 20 N.

increases from 4, for $T = 5$ N, to 5 for $T = 20$ N, see Figure 14. Note that the wrinkle wavelength decreases when the number of wrinkles increases, and the wrinkle amplitude is also observed to have decreased. These observations are consistent with the analytical model for the wrinkled region, Equation 25, and the wrinkle details, see Equations 31 and 32. The wrinkle amplitudes for symmetrical loading were found to be always very small, even at the higher load levels.

Afterwards, T_2 was maintained at 5 N but T_1 was increased up to a maximum load ratio of 4. Figure 15 shows the wrinkle profiles at three different cross sections, for different values of T_1/T_2, plotted against those obtained from the ABAQUS simulations.

Note that experiments and simulations match closely in the central region; particularly the wrinkle wavelengths are predicted accurately. But ABAQUS predicts larger displacements of the edges of the membrane, and this is due to the fact that the initial shape of the physical model has not been captured with sufficient accuracy. The edges of the membrane were initial curled due to residual stresses from the manufacturing process.

Validation of Analytical Model

In order to validate the analytical model for symmetric load cases compare, Table 1, the predictions for wrinkle wavelength and amplitude from Equations 30–32 with the experimental measurements in Figure 14.

For asymmetric load cases, Tables 2 and 3, compare the analytical predictions at the centre of the membrane for $T_1/T_2 = 4$ and two different membrane thicknesses, namely 0.025 mm and 0.05 mm, with predictions from ABAQUS and experimental measurements. Recall that in this case there is a single diagonal wrinkle, see Figure 15(c).

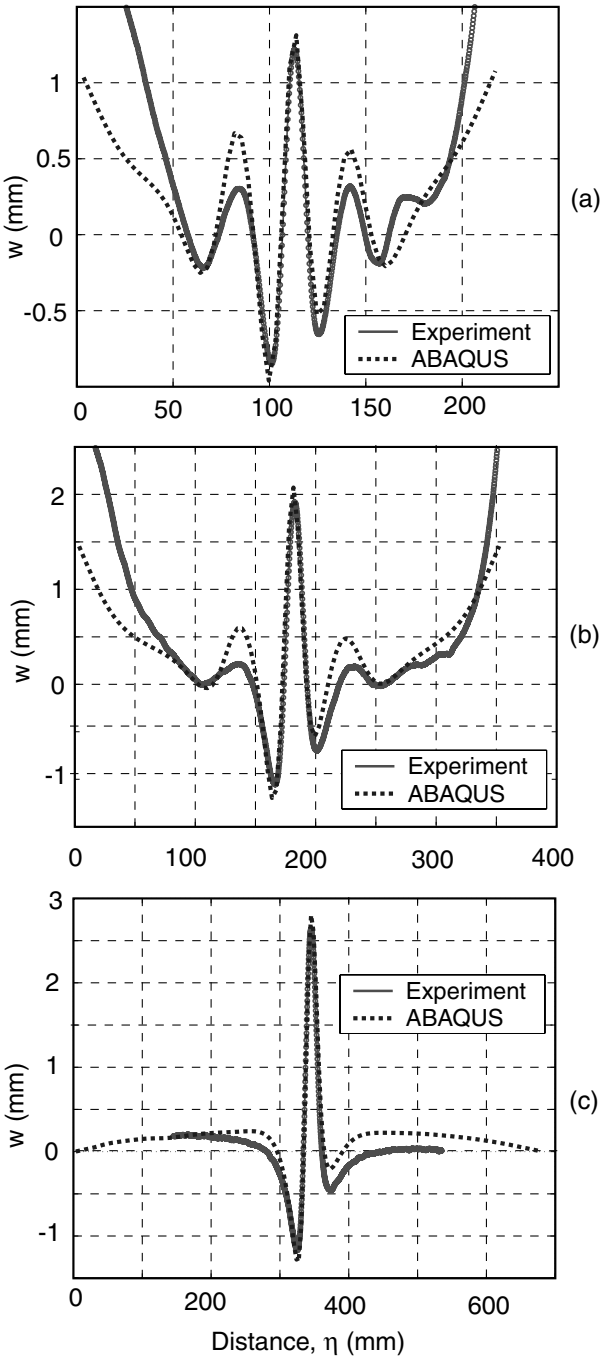

Fig. 15 Comparison of experimental measurements with ABAQUS for $T_1/T_2 = 4$ and cross sections at distance of (a) 105 mm, (b) 177 mm, (c) 346 mm from corner.

The predictions for the half-wavelength are very close to the experiments and FE analysis. For the wrinkle amplitudes, we have compared both the predictions using only analytical solutions, Equation 38 with δ_1 and δ_2 from Equation 17, or those based on Equation 38 but with corner deflections from a 2-D

[§]2-D IMP/ no-compression Analysis.
[¶]Shell model.

Table 1 Comparison of number of wrinkles, half-wavelength and amplitude for symmetric loading at 70 mm from corner

	$n/2$		λ (mm)		A (mm)	
T (N)	Eq. 30	Exp.	Eq. 31	Exp.	Eq. 32	Exp.
5	4.3	4	12.9	11.0	0.135	0.124
20	6.1	5	9.1	9.7	0.191	0.141

Table 2 Wrinkle half-wavelengths for $T_1/T_2 = 4$ at 346 mm from corner

t (mm)	Eq. 37 (mm)	Exp. (mm)	FE (mm)
0.025	24.7	25.4	22.3
0.050	41.5	33.9	35.6

Table 3 Average wrinkle amplitudes for $T_1/T_2 = 4$ at 346 mm from corner

t	Eqs 38, 17	Eq. 38+FE[§]	Exp.	FE[¶]
0.025	3.51	2.5	1.89	2.02
0.050	3.33	2.1	1.81	1.63

no-compression analysis. We can see that the fully analytical estimates are up to 85% higher than those measured experimentally. However, if we use the corner displacements δ_1 and δ_2 predicted by ABAQUS and substitute them into Equation 38, we obtain improved estimates only 32% and 16% higher than the measurements.

Discussion and Conclusions

Two wrinkling regimes have been identified for square membranes subject to four in-plane corner forces. The first regime occurs for symmetric and asymmetric loading up to $T_1/T_2 \approx 2.5$. It is characterised by relatively small, radial corner wrinkles. The second regime occurs for asymmetric loading with $T_1/T_2 > 2.5$, and is characterised by a single, large diagonal wrinkle, plus small radial wrinkles at all four corners.

We have proposed an analytical method for predicting wrinkle wavelengths and out-of-plane wrinkle displacements, plus the in-plane corner displacements of the membrane are also estimated by this method.

For symmetric loading of the membrane, the analytically predicted wrinkle wavelengths have been shown to be within 10% of experimental measurements and the amplitudes within 30%.

For asymmetric loading, the analytically predicted wrinkle wavelengths are within 22% of the measurements, but the amplitudes are up to 85% too high, unless the corner displacements predictions are refined by carrying out a two-dimensional FE analysis. If this is done, the modified analytical predictions are within 32% of measured values.

Finite element analysis using thin shell elements has been shown to be able to replicate real physical experimentation with an accuracy typically better than 20%. However, a very fine mesh had to be used to resolve the small corner wrinkles; hence a complete simulation takes up to several days on a 2GHz Pentium 4 PC.

While we have captured remarkably accurately the behaviour of these membranes using relatively simple models, curling of the edges of the membrane, due to residual stresses resulting from manufacturing, still needs to be quantified and modelled.

Finally, an important area that will need to be addressed next is the behaviour of very large membranes. While predictions can be made using the approach presented in this paper, the validity of our results has been tested only for 0.5 m length membranes; their validity for membranes that are one or two order of magnitudes larger remains to be verified.

Acknowledgments

We thank Professor C.R. Calladine for helpful suggestions. Partial support from NASA Langley Research Center, research grant NAG-1-02009, Integrated membranous-microelement space structures technology (technical monitor Dr. K. Belvin) is gratefully acknowledged.

References

[1]McInnes, C.R., "*Solar Sailing",* Springer and Praxis Publishing, 1999.

[2]Greschik, G. and Mikulas, M.M., "Design study of a square sail architecture", *Proc. 42nd AIAA/ASME/ASCE/AHS/ASC Structures, Structural Dynamics, and Materials Conference and Exhibit*, Seattle, WA, 16-19 April 2001, AIAA-2001-1259.

[3]Wong, Y.W. and Pellegrino, S., "Amplitude of wrinkles in thin membrane". *New Approaches to Structural Mechanics, Shells and Biological Structures*, (Edited by H. Drew and S. Pellegrino), Kluwer Academic Publishers, 2002.

[4]Wong, Y.W. and Pellegrino, S., "Computation of wrinkle amplitudes in thin membranes", *Proc. 42nd AIAA/ASME/ASCE/AHS/ASC Structures, structural Dynamics, and Materials Conference and Exhibit*, Denver, CO, 22-25 April 2002, AIAA-2002-1369.

[5]Calladine, C.R., "*Theory of shell structures",* Cambridge University Press, 1983.

[6]Hibbit, Karlsson and Sorensen, Inc., *ABAQUS Theory and Standard User's Manual*, Version 6.2, Pawtucket, RI, USA, 2001.

[7]Adler, A.L., Mikulas, M.M., and Hedgepeth, J.M., "Static and dynamic analysis of partially wrinkled membrane structures". *Proc. 41st AIAA/ASME/ASCE/AHS/ASC Structures, Structures Dynamics, and Material Conference and Exhibit*, Atlanta, GA, 3-6 April 2000, AIAA-2000-1810.